ChemComm

COMMUNICATION

View Article Online
View Journal | View Issue

Cite this: *Chem. Commun.*, 2025, **61**, 8071

Received 16th February 2025,
Accepted 22nd April 2025

DOI: 10.1039/d5cc00847f

rsc.li/chemcomm

A multi-stack porphyrin oligomer with three cleft-like cavities for efficient guest encapsulations†

Rabban Rabban, Dhanyashree Das, Dhrubajyoti Talukdar and Bappaditya Gole *

We report here the design and synthesis of a covalently linked stacked tetra porphyrin oligomer, which has been a challenging task so far. The interlinking phenanthroline units and several intramolecular H-bonds help the molecule to fold into a sheet-like structure with three cleft-like cavities that bind two electron-deficient guests with high binding constant.

Nature efficiently captures and transforms solar energy into chemical energy through photosynthesis, a vital process that sustains life on Earth. Since the elucidation of the mechanistic details of the photosynthetic process, substantial efforts have been devoted to mimicking these natural processes by creating artificial systems,[1] particularly to address the pressing demand for renewable energy. Structural studies of photosynthetic systems have provided valuable insights into the critical role of the protein matrix in organizing chromophores in an intricate arrangement, enabling efficient charge transfer and separation.[2] However, the *de novo* design of such complex systems remains a formidable challenge. As an alternative, chemists have developed simpler strategies to organize synthetic dyes, such as assembling them into aggregates,[3] incorporating them into oligonucleotide backbones,[4] and creating dye oligomers that fold and self-assemble through noncovalent interactions.[5] Among these, discrete dye oligomers featuring a defined number of stacked aromatic units have emerged as particularly intriguing. Their well-defined folding behavior allows precise control, enabling insights into the interactions of π-conjugated systems and offers opportunities to tune their photophysical properties for functional applications.[6] Recent studies have demonstrated that dye oligomers containing strongly dipolar aromatic units or alternating donor–acceptor moieties exhibit efficient folding driven by favorable electrostatic interactions.[7] Additionally, the folded structure offers multiple cavities, a challenging feature to achieve, with the potential to encapsulate complementary guests and facilitate charge transfer.[8]

Porphyrins, central to the natural photosynthetic systems, have attracted immense interest for their exceptional optical and electronic properties.[9] Stacked porphyrin oligomers are particularly appealing due to their broad solar light absorption and remarkable interchromophoric communication. These systems remain invaluable for applications in artificial light-harvesting systems, catalysis, host–guest interactions, and optoelectronics.[10] However, the covalent synthesis of multi-porphyrin stacks beyond trimers is not known as they pose significant synthetic complexities with reduced efficiency.[11,12]

Here, we demonstrate the design and synthesis of a stacked tetrameric porphyrin oligomer, **1**. To the best of our knowledge, this is a rare instance where a covalently linked four porphyrin stack has been achieved. The phenanthroline derivative has been considered as a turn unit, enabling the molecule to adopt a folded structure in solution facilitated by multiple intramolecular H-bonds between endocyclic phenanthroline nitrogen and amide –NHs. These intramolecular H-bonds are quite strong, and our previous studies showed that they were instrumental in the formation of strained [2+2] macrocycles.[13] Density functional theory (DFT) geometry optimization confirms a sheet-like structure with three cleft-like cavities that are suitable for encapsulating electron-deficient guests, such as 2,4,7-trinitrofluorenone (TNF) among several other planar guests.

The outline for the synthesis of **1** is given in Scheme 1. The detailed synthetic method can be found in the ESI.† In brief, the phenanthroline monoacid, **5**, and diacid, **7**, were prepared by controlled hydrolysis from the diester **4**. The porphyrin acid **6** was prepared in a two-step process. First, a standard acid chloride mediated amide coupling between **5** and monoamino porphyrin **2** and then ester hydrolysis under basic conditions afforded **6** with an overall 36% yield. The preparation of diamino porphyrin clip, **8**, was carried out by an amide coupling reaction between the preformed diacid chloride of **7** and

Biomimetic Supramolecular Chemistry Laboratory, Department of Chemistry, School of Natural Sciences, Shiv Nadar Institution of Eminence Deemed to be University, Greater Noida, Uttar Pradesh, 201314, India. E-mail: bappaditya.gole@snu.edu.in

† Electronic supplementary information (ESI) available. See DOI: https://doi.org/10.1039/d5cc00847f

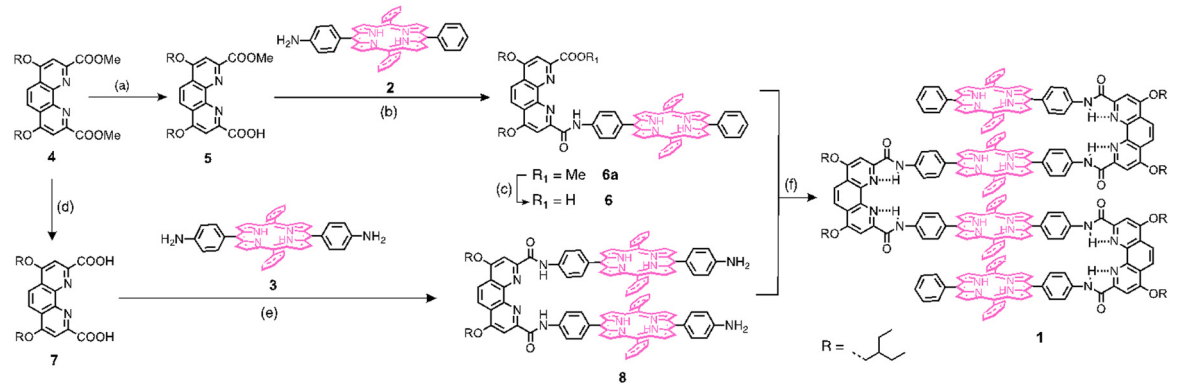

Scheme 1 Synthesis of tetrakis-porphyrin stack **1**. Conditions: (a) (i) KOH (1 equiv.), MeOH : THF (1 : 1), (ii) citric acid, 63%; (b) $(COCl)_2$, **2**, THF, DIPEA, 44%, (c) (i) NaOH, MeOH : THF (1 : 2), (ii) citric acid, 82%; (d) (i) KOH (3 equiv.), MeOH : THF (1 : 2), (ii) citric acid, 92%; (e) $(COCl)_2$, **3**, THF, DIPEA, 8%; (f) azabenzotriazole tetramethyl uronium hexafluorophosphate (HATU), pyridine, 18%.

the *trans*-diamino porphyrin **3**. This reaction was performed in a dilute condition with slow addition of the components to minimize oligomer formation. Finally, the condensation reaction between acid **6** and diamine **8** in a 2 : 1 ratio in pyridine using HATU gave **1** as a dark purple compound in an 18% yield. A detailed characterization of all these intermediates is provided in the ESI.†

The compound is well soluble in chlorinated solvents, but solubility drops drastically in more polar solvents. The characterization by NMR and MALDI-TOF mass spectroscopy confirms the formation of **1** (Fig. 1a and b; also see ESI†). The ^{1}H-NMR spectrum of the compound in $CDCl_3$ shows three amide –NH signals of equal intensities at around 11.5 ppm and two porphyrin pyrrole –NH peaks at −3.4 ppm and −3.9 ppm corresponding to three types of amides and two types of porphyrin –NH. This is consistent with the folded

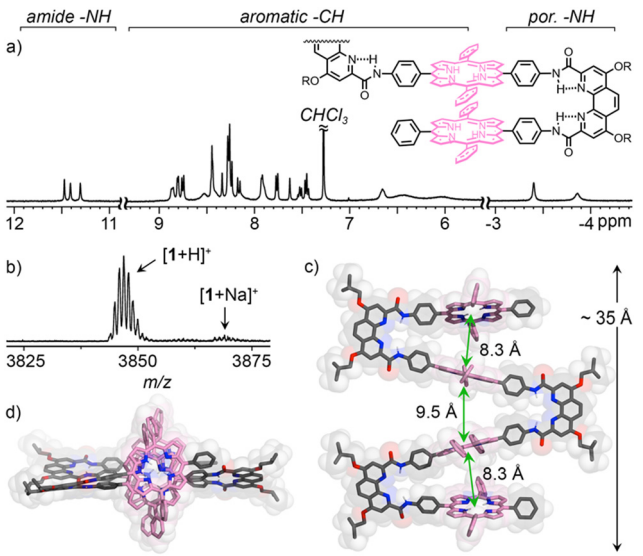

Fig. 1 (a) Selected region 400 MHz ^{1}H-NMR spectra of **1** (0.5 mM) in $CDCl_3$ at 298 K and its MALDI-TOF mass spectra (b). Side view (c) and top view (d) of the DFT optimized structures of **1** show the relative orientation of the porphyrin units with their center-to-center distances.

stacked structure, where a plane of symmetry can be imagined that separates the molecule into two parts. Thus, porphyrin –NH proton signals at −3.4 ppm and −3.9 ppm can be assigned to the outer and inner porphyrins, respectively. Apart from this, two types of aromatic protons were observed: a sharp set of signals between 9–7.5 ppm and another broad and unresolved set of signals at 7–5.7 ppm. The broad peaks shifted upfield can be attributed to the central porphyrins, which face a significant ring current. The broadness of the peaks, even below 0.12 mM in $CDCl_3$ (Fig. S1, ESI†), indicated some intramolecular conformational dynamics in the solution, particularly in the inner porphyrins. To ascertain this, a variable temperature (VT) NMR was performed in $C_2D_2Cl_4$ in a temperature range of 298 K to 373 K (Fig. S2, ESI†). The ^{1}H-NMR spectra in $C_2D_2Cl_4$ at 298 K are quite similar to what was observed in $CDCl_3$, without much noticeable change in the chemical shifts (Fig. S3, ESI†). Interestingly, the broad peaks started to become sharper once the temperature was raised, along with a significant downfield shift. However, the other sharp signals do not show any significant change during temperature variation. This behavior indicates that there might be some conformational rearrangement involved, which becomes faster at higher temperatures. The downfield shift may indicate that the two central porphyrins are probably initially in a slipped stacking arrangement that unfolds at higher temperatures. At lower temperatures up to 243 K, these signals gradually become much broader and shifted upfield (Fig. S4, ESI†), presumably due to the intermolecular interaction.

Since obtaining single crystals of **1** was unsuccessful, we have performed DFT geometry optimization (see ESI,† for more details) to get some structural information. The optimized structure showed that the geometry maintains a folded structure where intramolecular H-bonds between the phenanthroline endocyclic-N and amide-NH are prominent (Fig. 1c and Fig. S28, ESI†). Importantly, four porphyrin units are located on top of each other but not in an exact parallel orientation (Fig. 1d). They maintain a diverging angle of ∼25°. This is presumably to avoid steric interactions among the two phenyl rings close to the amide linkage. The center-to-center distances

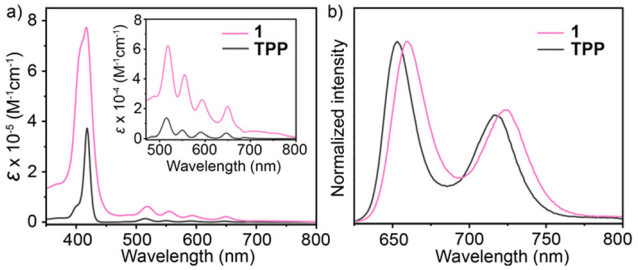

Fig. 2 (a) UV-vis spectra of **1** in $CHCl_3$ at 298 K, along with the spectrum of reference **TPP**. (b) Normalized fluorescence spectra of **1** and **TPP** in $CHCl_3$ (λ_{ex} = 515 nm).

between the porphyrin rings are not equal; the two peripheral distances (~8.3 Å) are similar and smaller compared to the central one (~9.5 Å). The large distances ruled out the existence of substantial π–π interactions among the porphyrin rings; however, the stacks have sufficient space for accommodating suitable guests in the clefts. Notably, the phenanthrolines and porphyrins maintain a near orthogonal orientation to adopt a folded structure, which was further confirmed by the correlation between two types of porphyrins –NH signals originated from outer and inner porphyrins as observed from NOESY NMR (Fig. S7, ESI†).

As expected, **1** displays several sharp, intense characteristic bands in the UV-Vis spectrum in chloroform (Fig. 2a). When compared with free-base tetraphenyl porphyrin (**TPP**), the absorption maxima for both the Soret band and Q-bands appeared nearly at a similar wavelength with some broadness in **1**. The molar extinction coefficient of **1** at 417 nm is nearly double (ε = 7.7 × 10^5 M^{-1} cm^{-1}) that of the **TPP** (ε = 3.7 × 10^5 M^{-1} cm^{-1}) with a broad Soret band. The broadness and blue shifted shoulder at 408 nm could be the result of the excitonic coupling between the porphyrin units that has been observed in other dimeric and trimeric porphyrin systems with varying interchromophore distances.[12] The variable concentration UV-Vis absorption spectra showed a linear variation of absorbance with a concentration range of 3.5–112 μM (Fig. S9 and S10, ESI†). Additionally, variable temperature absorption spectra of a 6.25 μM solution in the 303–343 K range in dichloroethane indicate no significant change in the spectrum (Fig. S11, ESI†). These results ruled out the existence of any molecular association at this concentration range. The fluorescence spectra of **1** in $CHCl_3$ showed an intense band at 660 nm and a vibronic band at 724 nm (Fig. 2b). Both these bands are red-shifted by 7 nm compared to **TPP**.

Considering the folded structure of **1**, it offers cleft-shaped cavities that can encapsulate guests. The planar electron-deficient guests were chosen, it being an electron-rich host. Therefore, we tested a series of guests with varying electron deficiency (Fig. 3a). The host–guest interaction was probed by UV-Vis and ^{1}H-NMR spectroscopy. For UV-Vis titration, a sub-micromolar concentrations of host **1** and guests were used. Among all the guests, we found that TNF (**G1**) had the strongest binding with the host (Fig. 3b). Upon the addition of **G1**, the absorbance of the Q bands at 518, 555, 593, and 650 nm

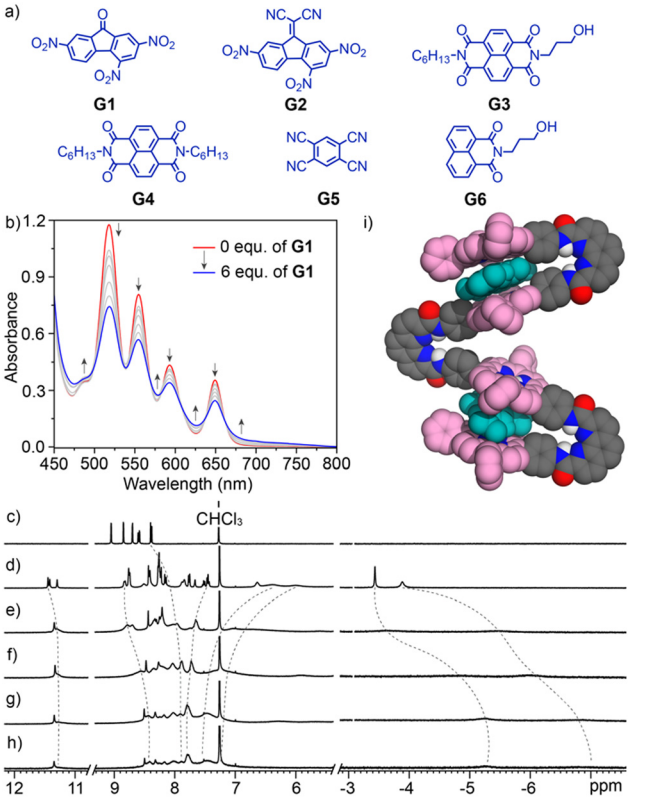

Fig. 3 (a) A series of electron-deficient guests were tested for the host–guest studies. (b) UV-Vis absorption spectra of **1** (50 μM) with the addition of **G1** (0–6 equivalents) in chloroform at 298 K. The selected region 400 MHz ^{1}H-NMR spectra of **G1** (10 mM) (c), **1** (1 mM) in $CDCl_3$ (d) and after the addition of 1 (e), 2 (f), 3 (g), and 4 equivalents (h) **G1** at 298 K. (i) Side view of the space-filling model of DFT energy minimized structures of **1**⊃**G1**$_2$ showing the relative orientation of the guests in the clefts. Nonpolar hydrogens and side chains are omitted for clarity.

diminished, and an increment of the absorbance at 488, 577, 626, and 684 nm was observed with clear isosbestic points at 498, 569, 582, 607, 637, and 662 nm. In contrast, no significant change was observed with other guests (Fig. S12–S16, ESI†). Furthermore, the Job plot revealed the formation of the 1 : 2 host–guest complex with **G1** (Fig. S17, ESI†) even though three clefts are available.

Upon gradual addition of **G1** to a solution of **1** in $CDCl_3$, the proton signals in ^{1}H-NMR become broad and shifted upfield (Fig. 3c–h). The porphyrin –NH protons were shifted from −3.4 to −5.3 ppm and −3.9 to −6.8 ppm before the host–guest complex precipitated out of the solution when a large excess of **G1** was added. While the sharp aromatic protons signal of **1** showed an upfield shift, the broad signals were shifted downfield, indicating that the conformation dynamics of the central porphyrins may be restricted upon guest binding. The complexation-induced chemical shifts and broadness of the peaks can be attributed to the presence of a strong shielding effect when guests interact with the porphyrin rings and the dynamic nature of the binding, which operates faster than the NMR time scale, respectively. The chemical shift variations were fitted using a 1 : 2 (H : G) binding model to obtain K_1 and

K_2 of 4.08×10^4 M^{-1} and 1.43×10^4 M^{-1}, respectively (Fig. S18, ESI†), to indicate a strong binding. The NMR titration with other guests revealed that **G2** and **G5** have some weak binding affinities with **1**, whereas **G3**, **G4**, and **G6** do not show any significant binding (Fig. S19–S25, ESI†). The estimated binding constants are summarized in Table S1 (ESI†). The differences in their binding can also be understood from the relative HOMO and LUMO energies of the guests compared to **1** (Fig. S26, ESI†).

Due to the lack of crystal structures and unresolved NMR signals, the detailed structural information of the host–guest complexation cannot be determined experimentally. However, we performed DFT energy minimization of the **1**⊃**G1**, **1**⊃**G1**$_2$, and **1**⊃**G1**$_3$ complexes to gain structural insights (Fig. S29–S31, ESI†). The sequential encapsulation of guests is energetically favorable, though the first complexation between **1** and **G1** is the most energetically preferred step (Fig. S27, ESI†) compared to subsequent steps. In particular, the third encapsulation, occurring between the two central porphyrins, is the least efficient. This is likely because, after two encapsulations, the two central porphyrins become the least electron-rich, further reducing their ability to accommodate a third guest. Additionally, the significant distance between the two central porphyrins limits their ability to bind guests effectively and engage in strong interactions. This is evident from the space-filling model of **1**⊃**G1**$_3$, where the two guests at the top and bottom cleft cavities are tightly packed, whereas the central guest is loosely bound (Fig. S31, ESI†). Overall, it corroborates the 1 : 2 host-to-guest binding from the UV-Vis and NMR experiments.

In conclusion, here we have demonstrated the design and synthesis of a rare covalently linked tetra porphyrin stacked oligomer. The phenanthroline unit was strategically used to provide several intramolecular H-bonds to help the molecule maintain a folded structure, even though some dynamics were observed between the two central porphyrin units, which was investigated by VT NMR. The well-organized folded structure offers three cleft-like cavities that encapsulate two electron-deficient TNF molecules with high binding constants. This novel system represents a significant advancement in developing multi-porphyrin oligomers, thus offering new opportunities for their potential applications in light-harvesting, energy conversion, photocatalysis, and molecular electronics. These objectives are being investigated, and the results will be reported in due course.

The authors acknowledge Shiv Nadar Institution of Eminence, Delhi NCR, and Anusandhan National Research Foundation (ANRF), Govt. of India (SRG/2022/000678) for financial support. DST-FIST scheme (SR/FST/CS-I/2017/13(C)) for MALDI facility.

Data availability

The data supporting this article have been included in the ESI.†

Conflicts of interest

There are no conflicts to declare.

Notes and references

1 T. Keijer, T. Bouwens, J. Hessels and J. N. H. Reek, *Chem. Sci.*, 2021, **12**, 50.
2 G. D. Scholes, G. R. Fleming, A. Olaya-Castro and R. Van Grondelle, *Nat. Chem.*, 2011, **3**, 763.
3 F. Würthner, C. R. Saha-Möller, B. Fimmel, S. Ogi, P. Leowanawat and D. Schmidt, *Chem. Rev.*, 2016, **116**, 962; M. Hecht and F. Würthner, *Acc. Chem. Res.*, 2021, **54**, 642; D. Bialas, E. Kirchner, M. I. S. Röhr and F. Würthner, *J. Am. Chem. Soc.*, 2021, **143**, 4500; M. Mahl, M. A. Niyas, K. Shoyama and F. Würthner, *Nat. Chem.*, 2022, **14**, 457; L. Rubert, H. M. A. Ehmann and B. Soberats, *Angew. Chem., Int. Ed.*, 2025, **64**, e202415774.
4 C. B. Winiger, S. M. Langenegger, G. Calzaferri and R. Häner, *Angew. Chem., Int. Ed.*, 2015, **54**, 3643; M. Vybornyi, Y. Vyborna and R. Häner, *Chem. Soc. Rev.*, 2019, **48**, 4347; F. D. Lewis, R. M. Young and M. R. Wasielewski, *Acc. Chem. Res.*, 2018, **51**, 1746.
5 S. Bhosale, A. L. Sisson, P. Talukdar, A. Fürstenberg, N. Banerji, E. Vauthey, G. Bollot, J. Mareda, C. Röger, F. Würthner, N. Sakai and S. Matile, *Science*, 2006, **313**, 84; A.-B. Bornhof, A. Bauza, A. Aster, M. Pupier, A. Frontera, E. Vauthey, N. Sakai and S. Matile, *J. Am. Chem. Soc.*, 2018, **140**, 4884; F. Würthner, *Acc. Chem. Res.*, 2016, **49**, 868; V. Dehm, M. Büchner, J. Seibt, V. Engel and F. Würthner, *Chem. Sci.*, 2011, **2**, 2094; S. Samanta, D. Mallick and R. K. Roy, *Polym. Chem.*, 2022, **13**, 3284.
6 E. Kirchner, D. Bialas, F. Fennel, M. Grüne and F. Würthner, *J. Am. Chem. Soc.*, 2019, **141**, 7428; D. Bialas, A. Zitzler-Kunkel, E. Kirchner, D. Schmidt and F. Würthner, *Nat. Commun.*, 2016, **7**, 12949; B. Gole, B. Kauffmann, A. Tron, V. Maurizot, N. McClenaghan, I. Huc and Y. Ferrand, *J. Am. Chem. Soc.*, 2022, **144**, 6894.
7 X. Hu, J. O. Lindner and F. Würthner, *J. Am. Chem. Soc.*, 2020, **142**, 3321; X. Hu, A. Schulz, J. O. Lindner, M. Grüne, D. Bialas and F. Würthner, *Chem. Sci.*, 2021, **12**, 8342; R. S. Lokey and B. L. Iverson, *Nature*, 1995, **375**, 303; A. Schulz, R. Fröhlich, A. Jayachandran, F. Schneider, M. Stolte, T. Brixner and F. Würthner, *Chemistry*, 2024, **10**, 2887.
8 Y. Ferrand and I. Huc, *Acc. Chem. Res.*, 2018, **51**, 970.
9 H. Lu and N. Kobayashi, *Chem. Rev.*, 2016, **116**, 6184; R. D. Mukhopadhyay, Y. Kim, J. Koo and K. Kim, *Acc. Chem. Res.*, 2018, **51**, 2730; P. S. Bols and H. L. Anderson, *Acc. Chem. Res.*, 2018, **51**, 2083.
10 H. Gholami, D. Chakraborty, J. Zhang and B. Borhan, *Acc. Chem. Res.*, 2021, **54**, 654; E. Nikoloudakis, I. López-Duarte, G. Charalambidis, K. Ladomenou, M. Ince and A. G. Coutsolelos, *Chem. Soc. Rev.*, 2022, **51**, 6965.
11 A. Dhamija, D. Chandel and S. P. Rath, *Chem. Sci.*, 2023, **14**, 6032; Z.-Q. Wu, X.-B. Shao, C. Li, J.-L. Hou, K. Wang, X.-K. Jiang and Z.-T. Li, *J. Am. Chem. Soc.*, 2005, **127**, 17460; T. Haino, T. Fujii, A. Watanabe and U. Takayanagi, *Proc. Natl. Acad. Sci. U. S. A.*, 2009, **106**, 10477; N. Hisano, T. Kodama and T. Haino, *Chem. – Eur. J.*, 2023, **29**, e202300107.
12 C. Schissler, E. K. Schneider, S. Lebedkin, P. Weis, G. Niedner-Schatteburg, M. M. Kappes and S. Bräse, *Chem. – Eur. J.*, 2021, **27**, 15202; M. Kasha, H. R. Rawls and M. A. El-Bayoumi, *Pure Appl. Chem.*, 1965, **11**, 371; L. Zanetti-Polzi, A. Amadei, R. Djemili, S. Durot, L. Schoepff, V. Heitz, B. Ventura and I. Daidone, *J. Phys. Chem. C*, 2019, **123**, 13094; S. Faure, C. Stern, R. Guilard and P. D. Harvey, *J. Am. Chem. Soc.*, 2004, **126**, 1253.
13 R. Rabban, J. M. Kumar, N. Karmodak and B. Gole, *New J. Chem.*, 2024, **48**, 1894.

